



Numerical investigation of gravity retaining wall foundation failure mechanisms

A. Kamalzadeh & M.J. Pender

The University of Auckland, Auckland, New Zealand.

ABSTRACT

This research investigates the response of the gravity retaining walls subjected to monotonic and sinusoidal loadings, adopting the OpenSees finite element analysis. Recent research has shown the capacity of the shallow foundation supporting the wall controls the behaviour of the system, Pender (2018). Understanding the wall system failure mechanism can help us in seismic resistant design of gravity wall systems. There has been a controversy in the geotechnical engineering community on whether the failure mechanism initiates by rotational deformation or horizontal sliding.

The appeal of utilising OpenSees is the capability of its available constitutive models for soil, particularly the Manzari-Dafalias which can represent the complete spectrum of drained behaviour of sand from very loose to dense (and also undrained behaviour and pore pressure response).

Cantilever walls with a reinforced concrete stem and base will be investigated to check on the rotational and sliding foundation failure mechanisms. The earthquake response of the system is likely to produce permanent deformations of the foundation soil beneath the heel and toe of concrete base of the wall. The implications of this for wall system performance under subsequent earthquakes will be investigated. Ricker Wavelet dynamic input motion will be applied to investigate the above factors.

1 INTRODUCTION

The current design approach can be traced back to 1g shaking table tests observations performed by Okabe (1924) and Mononobe and Matsuo (1929), the so-called M-O approach. With some modifications by Seed and Whitman (1970) the M-O method has become the main approach for designing earthquake-resistant retaining structures. The appeal of this method is its simple application. Formula 1 to 3 show how the M-O lateral thrust is calculated.

$$K_{AE} = \frac{\cos^2(\varphi - \theta - \alpha)}{\cos\theta \cos^2\alpha \cos(\alpha + \delta + \theta)(1 + \sqrt{\frac{\sin(\varphi + \delta)\sin(\varphi - \theta - i)}{\cos(\alpha + \delta + \theta)\cos(i - \alpha)}})^2}$$
(1)

$$\theta = tan^{-1} \left(\frac{k_h}{1 - k_v}\right) \tag{2}$$

$$P_{AE} = 0.5K_{AE}\gamma H^2 \text{ with } P_{AEh} = P_{AE}\cos\delta \text{ and } P_{AE\nu} = P_{AE}\sin\delta$$
 (3)

Where φ is the backfill friction angle, α is the angle between the backfill side of the wall with the vertical, δ is the interface friction angle, i is the backfill surface slope angle, γ is the unit weight of the backfill and, H is the height of the wall. Note that in the absence of a dynamic excitation ($\theta = 0$) therefore, we can calculate pressures induced by soil self weight.

Although, recent design approaches concludes the equivalent static seismic force distribution along the depth of the wall is similar to an inverted triangle, using centrifuge test and FE models some researchers currently found out it is an upright triangle (Mikola et al., 2014, Chin et al., 2016, Wood, 2018). Moreover, another source of overestimation is the equivalent force magnitude, especially where design PGA (peak ground acceleration) exceeds (Sitar et al., 2012). The current design method assumes maximum dynamic earth pressure is simultaneous with the wall peak inertia force causing over-conservative design while centrifuge test results have shown the occurrence time of these is not coincident (Sitar and Al Atik, 2008). Al Atik and Sitar (2010) have implemented finite element (FEM) analyses using the OpenSees (McKenna et al., 2013) platform (developed by The University of Berkley, California) to model their centrifuge tests and full-scale models. They find the FEM analyses results from OpenSees are in strong agreement with centrifuge test results and find the current design method is excessively conservative. Also, Chin et al. (2016) used OpenSees modelling and localised their models using typical New Zealand soil types and seismic zones of NZS 1170.5 (Standards New Zealand Technical Committee, 2004) for embedded cantilever walls with two different propping configurations.

In this study, we used OpenSees to model soil-retaining wall problem types. The GiD (Coll et al., 2016) pre/post-processing software, has been utilised to build the geometry of the model. The soil profile is assumed to have unlimited lateral extent, and there is a bedrock lying under the model. The wall dimensions are the same as one of the cases in Pender (2018) paper. The static and dynamic response of the wall is investigated.

2 BUILDING THE MODEL

2.1 Geometry and boundaries

The 2D soil – gravity cantilever retaining wall is modelled in the OpenSees (McKenna et al., 2013). The soil profile is assumed unlimited in the horizontal direction hence, only a small portion of it around the retaining wall is modelled which we call it the interior model. To establish an accurate model, the interior model has a mesh size of 10cm in the proximity of the retaining wall. However, the mesh becomes larger as we move on to the sides of the model.

All the soil elements are of a four-noded, quadrilateral, plane-strain type with a single robust integration point (Gauss point) and, two translational degrees of freedom (DOF) at each node. These elements are called SSPquad in the OpenSees. The interior model has a length of 80m, depth of 20m and 8m backfill on the left side, see Figure 1. Assuming the soil profile has large lateral extent, two blocks of soil columns have been

Paper 99 – Numerical Investigation of Gravity Retaining Wall Foundation Failure Mechanisms

modelled at both sides of the interior model. The out of plane thickness of these columns are significant, 10,000m, to represent the mass of the assumed infinite soil profile. Periodic boundary condition is simulated to ensure the vertical shear wave propagation in these soil columns. This means in a single soil column, the nodes at the same level, are tied together in both directions using the equalDOF command in the OpenSees as in Figure 2 (McGann and Arduino, 2015). The free-field columns are approximately situated at 40m distance from the wall to eliminate any influence that this boundary may have on the retaining wall area.

During the static analysis, the base of the model is fixed in both directions while throughout the dynamic analysis the vertical DOF is fixed.

The gravity cantilever retaining wall is simulated using two-node elastic beam-column elements with two translational DOFs and a rotational one at each node. This wall is considered to be reinforced concrete with an elastic modulus of 30 GPa and a density of 2.3 t/m³. The weight of the wall is applied at each node. The dimensions of the wall are similar to one of the Pender (2018) examples: 8m in height, 5m long foundation, 3m heel length, and all components 0.5m thickness.

The interfaces between the wall and soil nodes have two main characteristics. They can only behave in compression in their local axial axis, i.e. they should detach in case of tension and, their local lateral behaviour should be frictional. For this purpose, Flat Slider Bearing elements incorporated with simple Coulomb friction model has been utilized. The chosen stiffness of the element in the frictional direction is 3900 KPa (Drumm and Desai, 1986) and the axial stiffness is the outcome of trial and error based on the recommendations of Chin et al. (2016) and Kolay et al. (2013). The interface friction angle is equal to the underlying soil friction angle ($\delta/\varphi_{Soil}=1.0$) under the foundation. In addition, to prevent any impact effect during the dynamic analysis caused by partial uplift of the foundation or detachment of wall stem, a damping of five percent is incorporated in the axial behavior of the interfaces. It should be noted that the Rayleigh damping of the main system, does not have any effect on the interfaces.

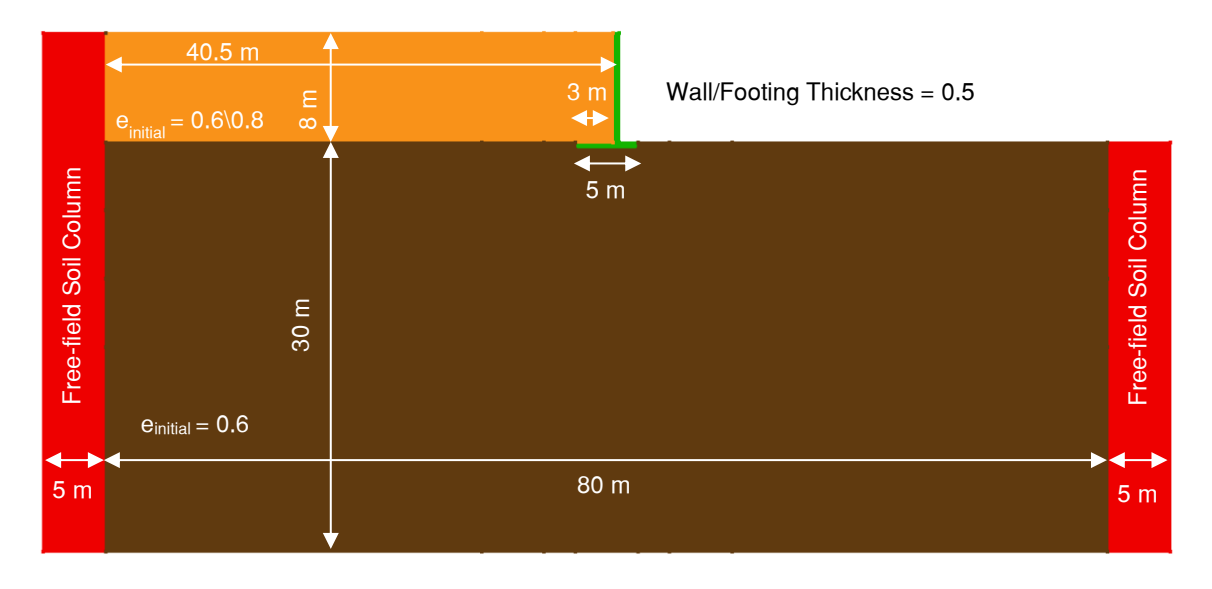


Figure 1: Retaining wall model geometry

2.2 Soil Material

OpenSees database offers a variety of constitutive models to represent the soil. Our objective is to model dry cohesionless soil. Therefore, Manzari and Dafalias constitutive model (Dafalias and Manzari, 2004) employed. Manzari and Dafalias soil model is capable of modelling the cohesionless soil plasticity, cycling and dilative behaviour. The appeal of using Manzari and Dafalias over other constitutive models is its ability to show the peak shear strengths (not to confuse with the ultimate/critical shear strength at large strains) of

Paper 99 – Numerical Investigation of Gravity Retaining Wall Foundation Failure Mechanisms

dry sands at low confining pressures. Pender and Kamalzadeh (2019) contains the behaviour of the materials in Table 1 in a drained triaxial condition. This can be interesting as the mean stress in the backfill and the underlying soils in our problem type would probably be of low values as we don't have any surcharge on the backfill.

The soil properties used in this study are derived from Dafalias and Manzari (2004) for Toyoura sand. The denseness of the soil in the Manzari and Dafalias constitutive model can be defined by the initial void ratio (e_o), the higher e_o, the softer the soil. See Table 1 for the main soil properties. As can be seen, the underlying soil is dense and, the backfill is relatively looser. We select the dilatancy values for the looser material close to zero to turn off the dilatant behaviour of this type of soil.

Table 1: Main soil Properties

	Unit	Dense Dilatant Sand	Medium Non-Dilatant Sand	Bedrock
Depth	m	20.0	8.0	∞
Density (ρ)	t/m^3	2.0	1.9	2.4
Shear Wave Velocity (Vs)	m/s	148	132	1800
Initial Void Ratio (e _o)	-	0.6	0.8	-
Initial Shear Modulus (G _o)	MPa	43.9	32.7	-
Friction Angle (φ)	degrees	42	33	-
Static Poisson's Ratio (v _{st})	-	0.30	0.30	-
Dynamic Poisson's Ratio (v _{dyn})	-	0.05	0.05	-

We investigated two main cases in this study, for both cases the 30m deep soil and the backfill soil materials are of dense dilatant and medium non-dilatant respectively:

- 1. A wall with 3m heel as shown in Figure 1.
- 2. A wall with the same foundation width in Figure 1 (5m) but with no heel, i.e., L-shaped wall.

2.3 Staged construction

To re-enact the real conditions of a cantilever retaining wall construction, we analysed the model in two stages for the in-situ conditions to take into place:

- 1. The 30 m deep is subjected to its gravity loads
- 2. The backfill and the wall is constructed and then the whole model is analysed for the gravity loads corresponding to that.

The effect of the first stage on further deformations and strains has been ruled out.

2.4 Dynamic excitation and boundaries

A Ricker wavelet, has been used as the acceleration excitation input. Ricker wavelet excitation (Fardis et al., 2003, Loli et al., 2015), both as a single event and as a series of repeated wavelets, is used, rather than earthquake time history, as this gives a clearer indication of how the wall system is responding. The attraction of utilising this particular wavelet is the pulse-like shape of the wave and, the simplicity of interpreting the model response comparing to an earthquake record. The equation of this artificial wavelet is given by:

$$f(b,t) = [6b - 24b^{2}(t - t_{o})^{2} + 8b^{3}(t - t_{o})^{4}]e^{-b(t - t_{o})^{2}}$$

$$\tag{4}$$

$$b = (\pi f)^2 \tag{5}$$

Where t is time, t_0 is the time at which the Ricker wavelet magnitude is maximum, and f is the frequency. The magnitude of the input Ricker wavelet is then modified to reach a desired value of acceleration. Using a

Paper 99 – Numerical Investigation of Gravity Retaining Wall Foundation Failure Mechanisms

series of site response analyses have been done on a 1D soil column with a depth of 20m in OpenSees, a proper value for the frequency of the Ricker wavelet has been chosen. See a normalized Ricker wavelet acceleration time history in Figure 2a.

As for the boundaries during dynamic excitation, all the nodes at the base (slave) are tied to the bottom left corner node (master) horizontally. To avoid trapping the shear waves in the system, a zero-length dashpot with a viscous material at the bottom left corner, known as Lysmer-Kuhlemeyer dashpot (1969), is used to play the role of the elastic half-space beneath the model, see Figure 2b. While one end of the dashpot is fixed in both directions, the other end is tied horizontally to the master soil node at the bottom left corner. Employing Joyner and Chen (1975) approach, the viscous material damping coefficient is the product of mass density and shear wave velocity of the presumed elastic half-space underneath the model. This elastic half-space is a bedrock with the properties in Table 1.

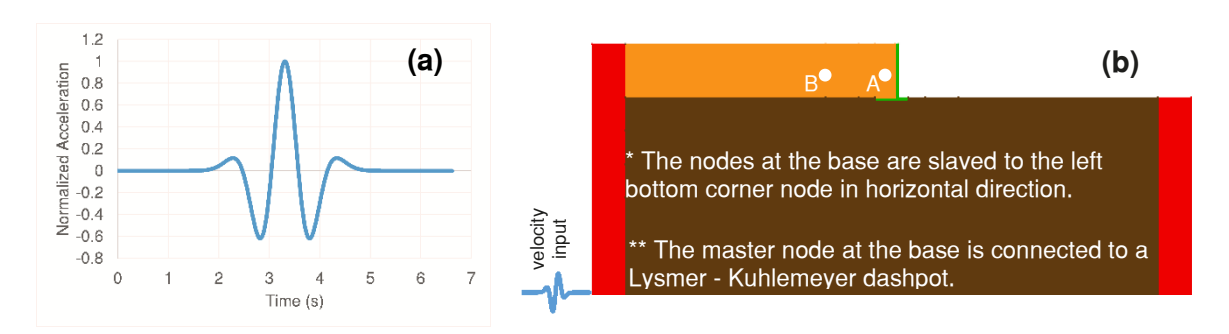


Figure 2: (a) Ricker wavelet normalized Acceleration time history, (b) Schematic point of application of the Ricker wavelet in velocity form

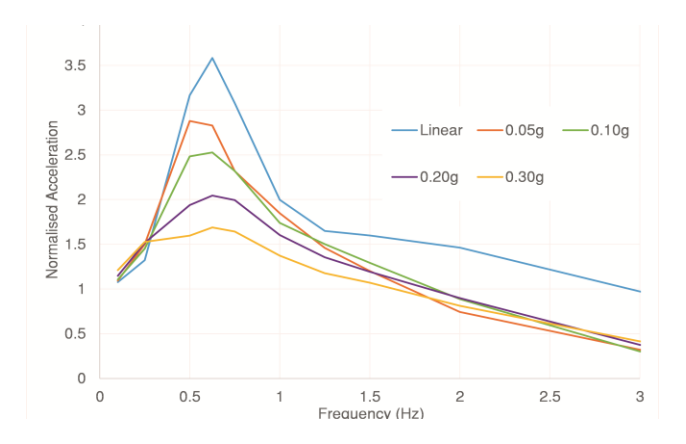


Figure 3: Acceleration site response of the 1D soil column

3 RESULTS AND DISCUSSION

3.1 Site response

To achieve the maximum acceleration amplification behind the wall caused by the Ricker Wavelet input, we conducted site response analyses on a 1D soil column. This 1D soil column has the same geometry of the left-side free-field soil column in Figure 1. The void ratio of the column is 0.6 and 0.8 for the first 30m and 8m on top respectively. The soil material is the same as the second case in section 2.2. The outcome is the normalised acceleration response spectrum at in Figure 3. Figure 3a is showing the normalised peak ground acceleration is almost at its highest point in the vicinity of f = 0.625 Hz. Therefore, we selected Ricker wavelet inputs with this frequency for dynamic analysis in this study.

Paper 99 – Numerical Investigation of Gravity Retaining Wall Foundation Failure Mechanisms

3.2 Gravity analysis

The results for the gravity analyses (stage 2 of section 2.3) can be seen in Figure 4 for the 3m heel and L-shaped wall. The OpenSees outputs are fed to the GiD software to generate contours in Figure 4a and 4b. Bear in mind that positive and negative volumetric strains show increase and decrease in volume respectively. Figure 4a indicates volume decrease in the backfill behind the wall. However, Figure 4b indicates volume the traditionally accepted triangular wedge in the backfill. With lateral displacement of wall top to be 0.16% and 0.34% of the wall height for 3m heel and L-shaped wall respectively, one would expect the formation of an active pressure distribution (Clough and Duncan, 1991). Figures 3c and 3d manifest the lateral pressure distributions against the virtual back of the wall with similar magnitudes for both cases. The earth pressure distributions for the 3m heel wall are a little larger than the L-shaped wall. The maximum earth pressure is happening at 1m height of the 3m heel wall whereas, this maximum is at the base of the wall for the L-shaped case.

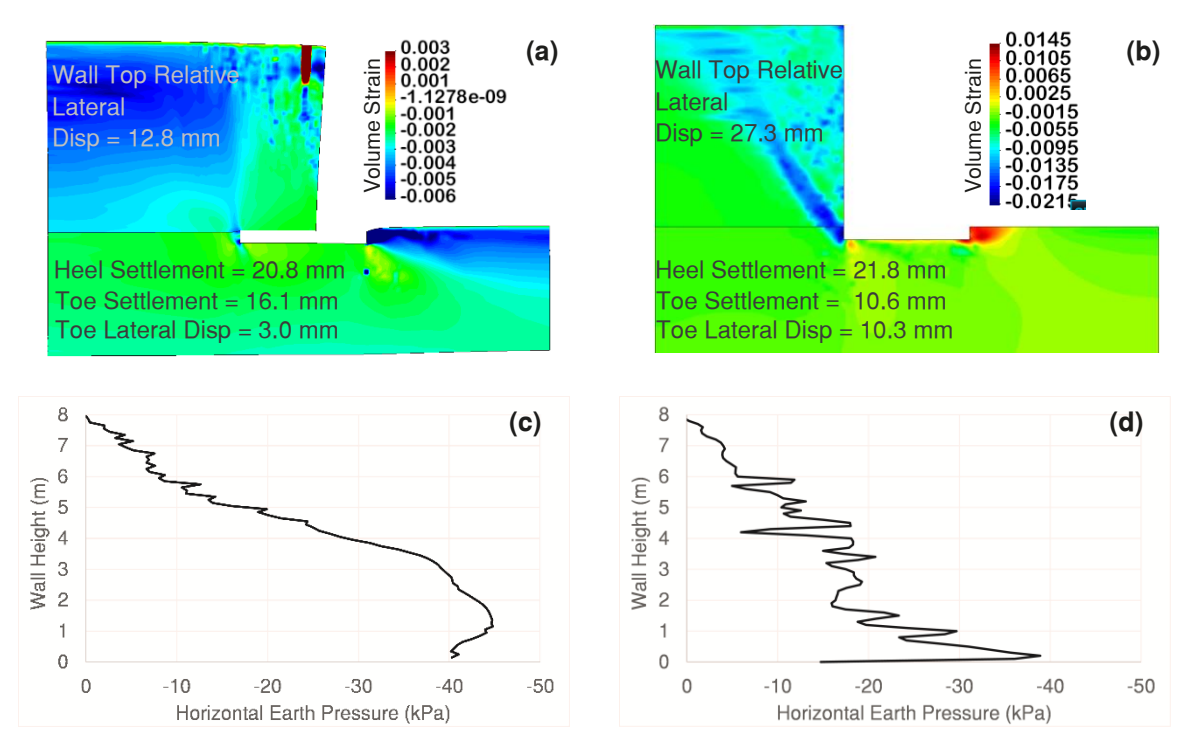


Figure 4: Cantilever retaining wall gravity results. (a) and, (b) deflected shape and volumetric strain of the foundation for 3m heel and L-shaped wall respectively, (c) and, (d) lateral earth pressure distribution for 3m heel and L-shaped wall respectively.

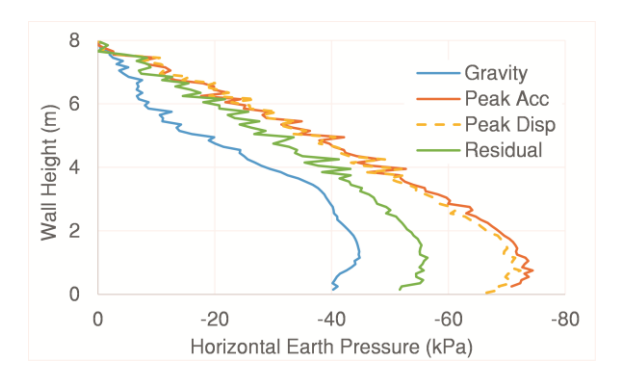
The critical friction angle for this sand gives us a value of 0.32 for the K_a while, the mobilised earth pressure coefficients corresponding to Figures 3c and 3d are 0.38 and 0.27 respectively. Despite the L-shaped wall, there is no evidence of distinctive shear failure zone can be observed as suggested by active earth pressure theory for the 3m heel wall. Looking closer at the rotation of wall foundation in both cases, a counterclockwise movement can be seen. This may be another contributing factor in the difference between existing and conventional active pressure distributions.

3.3 Dynamic Analysis

The walls responses to a single Ricker wavelet excitations is illustrated in Figures 5 to 7. The peak horizontal accelerations for the 3m heel and L-shaped wall generated behind the wall stem were 0.31g and 0.20g respectively. Figure 5 indicates the lateral earth pressure distributions against the virtual back of the wall. As one would expect, the excitation increased the earth pressures and there is little to no difference between the

Paper 99 – Numerical Investigation of Gravity Retaining Wall Foundation Failure Mechanisms

distributions at the peak acceleration and peak lateral displacement. While the 3m heel wall illustrates the residual lateral earth pressure distributions are higher than the static ones, there is no sign of this for the L-shaped case.



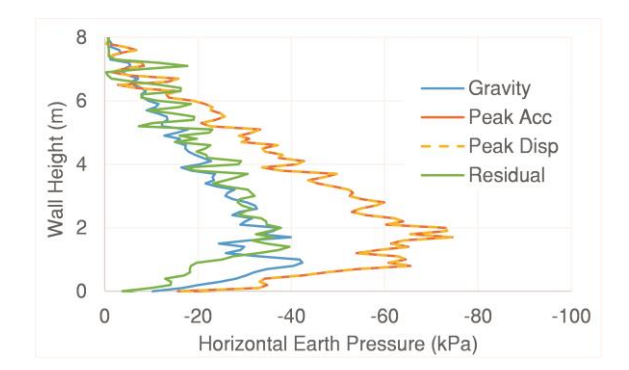


Figure 5: Lateral earth pressure distribution against the virtual back of the wall at different stage of the analysis for (a) 3m heel, (b) no heel

It should be noted that for Figures 7 and 8, all deformations and strains are due to the weight of the backfill and the Ricker wavelet excitation effect on the whole model, i.e., the effect of underlying soil is subtracted from these results (see section 2.3). However, it was noted that with the foundation layer in place, a certain amount of settlement of the layer occurred when the in situ gravity stresses were generated. Then if the 30 m deep layer, without the wall and backfill, is subject to Ricker wavelet excitation there will be more settlement. Under additional Ricker wavelet excitation additional settlement was observed, at least for the second and third excitations. Consequently, the settlement contours in Figures 6b and 7b include contributions from the rocking effect of the wall and backfill as well the additional settlement of the foundation layer from the Ricker wavelet.

As far as horizontal displacement and settlement are concerned Figures 6a and 6b show no special effect associated with the virtual back of the wall (a vertical line between the heel and the ground surface above). The same can be said of Figures 6c and 6d. It is apparent that there are concentrations of volumetric strain (dilatant volume increase) and shear strain in front of the toe of the foundation. Similar to the gravity results, Figures 7a, 7c and 7d indicate the presence of the conventional triangular wedge behind the wall.

4 CONCLUSIONS

This study has drawn the following conclusion:

- The conventional pseudo-static approach is distinctively different from the backfill response of the 8 m tall gravity cantilever wall with a 3 m wide heel in this study (Figures 6).
- The earth pressure distribution has an arch-shaped over the height of the wall. It increases linearly for upper part of the wall but for the lower part, it decreases.
- The residual lateral earth pressure distributions after the Ricker wavelet excitation are greater than the gravity pressure distributions for the 3m heel wall but not for the L-shaped one.
- A common approach to pseudo-static gravity wall design is to assume the boundary of the wall system is defined by a vertical interface rising upwards through the heel of the wall (virtual back); the backfill above the heel projection is assumed to be fixed to the wall. No evidence of the virtual back is seen in the finite element results for the 3m heel wall, except, perhaps, in the lateral displacement contours (Figures 6a).

Paper 99 – Numerical Investigation of Gravity Retaining Wall Foundation Failure Mechanisms

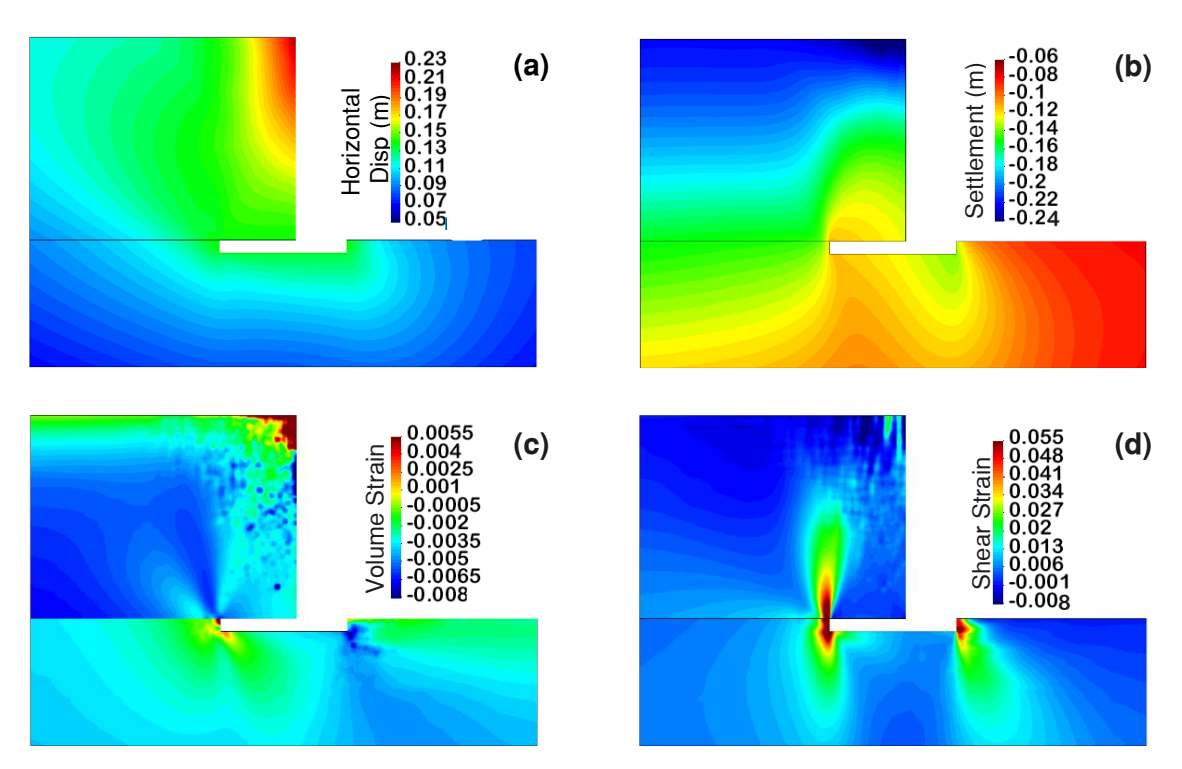


Figure 6: For 3m heel wall at peak lateral earth thrust: contours of (a) horizontal displacement, (b) settlement, (c) volumetric strain and, (d) shear strain

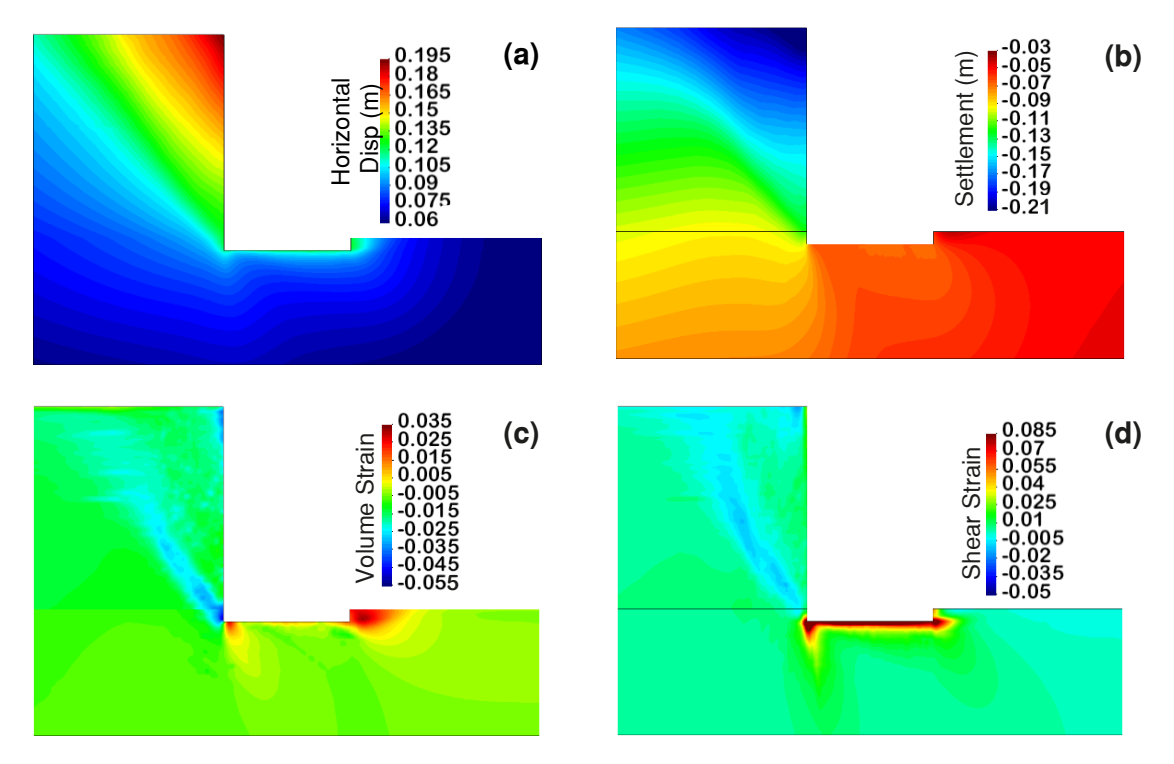


Figure 7: for no heel wall at peak lateral earth thrust: contours of (a) horizontal displacement, (b) settlement, (c) volumetric strain and, (d) shear strain

5 ACKNOWLEDGMENTS

The work of the second named author was funded by the University of Canterbury Quake Centre (UCQC). All the analyses have been done through the Mahuika platform of New Zealand e-Science Infrastructure

Paper 99 – Numerical Investigation of Gravity Retaining Wall Foundation Failure Mechanisms

(NeSI). The helpful advice of Dr Christopher McGann, Dr Alborz Ghofrani and, Mr Yuri Wong on aspects of the OpenSees software is greatly appreciated.

6 REFERENCES

- Al Atik, L. & Sitar, N. 2010. Seismic Earth Pressures on Cantilever Retaining Structures, *Journal of Geotechnical and Geoenvironmental Engineering*, Vol 136 1324-1333.
- Chin, C.Y., Kayser, C. & Pender, M. 2016. SEISMIC EARTH FORCES AGAINST EMBEDDED RETAINING WALLS: INSIGHTS FROM NUMERICAL MODELLING, *Bulletin of the New Zealand Society for Earthquake Engineering*, Vol 49 200-210.
- Clough, G. & Duncan, J. 1991. Earth pressures, Foundation engineering handbook. Springer.
- Coll, A., Ribo, R., Pasenau, M., Escolano, E., Perez, J.S., Melendo, A., Monros, A. & Ga, R.J. 2016. *GiD v.13 User Manual* [Computer Software].
- Dafalias, Y.F. & Manzari, M.T. 2004. Simple Plasticity Sand Model Accounting for Fabric Change Effects, *Journal of Engineering Mechanics*, Vol 130 622-634.
- Drumm, E.C. & Desai, C.S. 1986. Determination of parameters for a model for the cyclic behaviour of interfaces, *Earthquake Engineering & Structural Dynamics*, Vol 14 1-18.
- Fardis, N., Georgarakos, P., Gazetas, G. & Anastasopoulos, I. 2003. Sliding Isolation of Structures: Effect of Horizontal and Vertical Acceleration, *Fib International Symposium on Concrete Structures in Seismic Regions, 2003 Athens, 6–8 May.*
- Joyner, W.B. & Chen, A.T.F. 1975. Calculation of nonlinear ground response in earthquakes, *Bulletin of the Seismological Society of America*, Vol 65 1315-1336.
- Kolay, C., Prashant, A. & Jain, S.K. 2013. Nonlinear Dynamic Analysis and Seismic Coefficient for Abutments and Retaining Walls, *Earthquake Spectra*, Vol 29 427-451.
- Loli, M., Knappett, J.A., Anastasopoulos, I. & Brown, M.J. 2015. Use of Ricker motions as an alternative to pushover testing, *International Journal of Physical Modelling in Geotechnics*, Vol 15 44-55.
- Lysmer, J. & Kuhlemeyer, R.L. 1969. Finite dynamic model for infinite media, *Journal of the Engineering Mechanics Division*, Vol 95 859-878.
- McGann, C.R. & Arduino, P. 2015. *Dynamic 2D Effective Stress Analysis of Slope* (http://opensees.berkeley.edu/wiki/index.php/Dynamic_2D_Effective_Stress_Analysis_of_Slope). [Accessed 29 August 2017].
- Mckenna, F., Mazzoni, S. & Fenves, G. 2013. *Open System for Earthquake Engineering Simulation (OpenSees) Software Version 2.5.0* [Computer Software]. University of California, Berkeley, CA. Available from http://opensees.berkeley.edu.
- Mikola, R.G., Candia, G. & Sitar, N. 2014. Seismic earth pressures on retaining structures and basement walls, *Tenth US national conference on earthquake engineering, frontiers of earthquake engineering, Anchorage, Alaska, 2014.*
- Mononobe, N. & Matsuo, H. 1929. On the determination of earth pressures during earthquakes, *World Engineering Congress*, 1929 Tokyo, Japan.
- Okabe, S. 1924. General theory on earth pressure and seismic stability of retaining wall and dam. *J. of Japan Society of Civil Engineers*, Vol 10 1277-1323.
- Pender, M.J. 2018. Foundation design for gravity retaining walls under earthquake, *Proceedings of the Institution of Civil Engineers Geotechnical Engineering*, https://doi.org/10.1680/jgeen.17.00233.
- Pender, M.J. & Kamalzadeh, A. 2019. Insights from advanced numerical modelling into the pseudo-static design of gravity retaining walls, 7th ICEGE, Rome, Italy.
- Seed, H.B. & Whitman, R.V. 1970. Design of Earth Retaining Structures for Dynamic Loads, ASCE Specialty Conference, Lateral Stresses in the Ground and Design of Earth Retaining Structures, 1970 Cornell Univ., Ithaca, New York, 103-147.
- Sitar, N. & Al Atik, L. 2008. Dynamic centrifuge study of seismically induced lateral earth pressures on retaining structures, *Geotechnical Earthquake Engineering and Soil Dynamics IV*.
- Sitar, N., Mikola, R.G. & Candia, G. 2012. Seismically induced lateral earth pressures on retaining structures and
- Paper 99 Numerical Investigation of Gravity Retaining Wall Foundation Failure Mechanisms

basement walls, Geotechnical Engineering State of the Art and Practice: Keynote Lectures from GeoCongress 2012.

Standards New Zealand Technical Committee. 2004. Structural design actions (NZS 1170.5: 2004). Wellington, New Zealand.

Wood, J.H. 2018. Earthquake design of flexible soil-retaining structures, *Proceedings of the Institution of Civil Engineers - Geotechnical Engineering*, https://doi.org/10.1680/jgeen.17.00192.